Polymer Testing 119 (2023) 107930

Contents lists available at ScienceDirect

Polymer Testing

journal homepage: www.elsevier.com/locate/polytest

Experimental analysis at different loading rates of 3D printed polymeric auxetic structure based on cylindrical elements

D. Varas [a,*], J. Pernas-Sánchez [a], N. Fjeldberg [b,a], J. Martín-Montal [a]

[a] Department of Continuum Mechanics and Structural Analysis, University Carlos III of Madrid, 28911 Leganes, Madrid, Spain
[b] Department of Mechanical Engineering, Østfold University College, 1757 Halden, Norway

ARTICLE INFO

Keywords:
Auxetic structure
Dynamic regime
Split Hopkinson Pressure Bar
Additive manufacture

ABSTRACT

This work proposes the experimental study of an auxetic polymeric structure manufactured by 3D printing (SLA). The structure is composed by a re-entrant unit cell based on cylindrical elements not previously studied. The effect of the number and size/scale of the unit cells used in the specimens, subjected to both static and dynamic loads, has been analysed. The results show how the studied variables affect the behaviour of the structure in terms of stress and strain and that the dimensions of the cylindrical elements, as well as the contact between them, could help to modify the stiffness structure as required. The tests performed have allowed to understand the sequence of physical phenomena that appears at different strain rates and how they affect the response of the structure. The results obtained may contribute to the knowledge of both polymeric auxetic structures and the use of additive manufacturing methods for such structures.

1. Introduction

The engineering and technological sectors are constantly searching and demanding stronger, lighter, tougher, cheaper and more ductile materials that should have a strong combination of multiple material properties. Composite materials are a step in the right directions concerning those criteria's, however, they do not fully fulfil the increasing need for better materials. Metamaterials (also known as supermaterials) are a solution to these demands, as they are engineered to have properties not found in naturally occurring materials. One of those novel solutions are the auxetic structural materials, which could be designed to provide the required properties for certain applications.

An auxetic material is in simple terms a material with a negative Poisson's ratio. This means that, unlike most of the materials, they expand in the lateral direction when stretched in the longitudinal direction, and contract laterally under uniaxial compression. This behaviour provides them with an excellent shear strength [1,2], indentation resistance [1], high fracture toughness [3,4] and a high energy dissipation capacity [5,6] which makes them especially suitable to certain applications such as shock absorbers, filters, or biomedical implants, and can offer an enhanced protection for a large number of elements, structures and devices [7–11].

For more than 100 years, the existence of materials or structures with negative Poisson's ratio has been known in nature, such as pyrite single crystals, the skin of certain animals or cells and tissues of the human body [12,13]. However, it was not until 1986 when Lakes [1] proposed a method for obtaining a polymer foam with a re-entrant structure and negative Poisson's ratio. This type of material was called auxetic [14]. From that moment on, a great interest arose among the scientific community in the study of these materials, demonstrating that they possess excellent properties and that they can be candidates for a great variety of applications. One of the main problems that appeared when studying this type of materials was the difficulty of manufacture. The auxetic behaviour of these materials is due to the geometry of the unit cells of which they are composed, and the foams used presented as main disadvantage the difficult control in the definition of the unit cell of the foam, as well as its homogeneity. This fact prevented further development in the applications of these structures or materials, since their experimental behaviour did not always match with the available analytical and numerical models. However, recent developments in the field of additive technology constitute a turning point in the feasibility of fabrication of this typology of structures, which are unapproachable by conventional fabrication processes, allowing to avoid the aforementioned difficulties [15,16].

Among the possible applications of auxetic structures is their use as a protective element capable of absorbing a large amount of energy. The study and understanding of the behaviour of auxetic structures under different types of loads is essential for the development and design of auxetic protections. The key to the behaviour of a cellular auxetic (2D auxetic) or reticular (3D auxetic) structure is the unit cell,

* Corresponding author.
E-mail address: dvaras@ing.uc3m.es (D. Varas).

https://doi.org/10.1016/j.polymertesting.2023.107930
Received 19 October 2022; Received in revised form 15 December 2022; Accepted 5 January 2023
Available online 11 January 2023

as it is the basic structure that makes it up and which will define its mechanical properties. Its modelling has been approached mainly from two different methodologies, analytical and numerical, both being very useful to carry out preliminary analyses that help to design a unit cell that meets the desired requirements. Analytical models have been used by several researchers to acquire a deeper understanding of the design of these structures [16–20], as they allow relating the auxetic behaviour with various geometrical parameters of the cells. This approach can give satisfactory results in predicting their mechanical properties if boundary effects are adequately considered. Numerous studies have also been carried out using numerical techniques, such as finite element analysis, to predict the mechanical behaviour of these structures. It must be said that, in general, the studies performed had been focused on the study of small deformation elastic properties of metallic structures with two-dimensional auxetic behaviour, particularly the elastic moduli and Poisson's ratio [21–24]. In order to develop auxetic structures with high energy capacity and low force transmission, it is necessary to study also the large deformation range of these structures. However, studies on the mechanical behaviour of auxetic structures in this range are not as numerous as in small deformations and focus on numerical simulations of both foams and honeycombs with 2D re-entrant cells [25–29].

Regarding experimental works, it is worth to mention that different studies have been developed to analyse the behaviour of auxetic foams under compression, traction, shear and indentation in a quasi-static regime [30–34]. In addition to quasi-static studies, there are some works that study the behaviour of auxetic and sandwich foams with auxetic core, both at low or medium velocity and impact [35–40], concluding that these foams are good candidates for use as protection elements, as they have a high capacity for energy absorption and attenuation of the peak force. The improvement of the performance of auxetic foams for use as shielding elements could be achieved by modifying the unit cell of the auxetic structure by using precise geometries and parameters, which is very difficult. However, advances in additive manufacturing make it possible to produce auxetic structures with more complex cell architectures that can fulfil the design requirements for certain applications.

In the last years, and as a result of the possibilities offered by new additive manufacturing technologies, experimental works have been carried out to analyse the behaviour of auxetic structures with different kind of cells (re-entrant, arrowhead, chiral or inverted tetrapods) [35,41–46]. It must be said that most of the experimental works using auxetic structures manufactured by 3D printing are focused on quasi-static studies of metallic auxetic structures. In these studies, the influence of the different cell types and their geometric parameters upon the behaviour of the structure is observed, which, in combination with the material used in the manufacture, must be taken into account for the design and usage of these structures in certain applications.

Studies in dynamic regime of printed structures with 3D auxetic behaviour are really scarce [35,38,40,47,48] and however they are essential if we want to use them as impact protection elements, since the performance of these structures under dynamic loads can be radically different to that shown in quasi-static regime. In general, it has been observed that the behaviour of these structures depends on the strain rate and that the material used influences the different failure modes and, therefore the energy absorption capacity. Zhang and Lu [49] in 2020 studied an aluminium alloy auxetic structure under dynamic tensile loads and one of the main conclusions extracted is that the uniform deformation observed in quasi-static tension changes to localized deformation and wavelike propagation due to inertia effect under dynamic tension.

As it has already been mentioned, auxetic structures can provide interesting behaviours for many applications by achieving optimal properties. However, it must be said that in general, auxetic structures have a low stiffness, or at least a lower stiffness than the solid material from which they are formed due to their more porous structure. When an auxetic structure is compressed, the internal structure is gradually compacted. Therefore, the stress–strain curve has a much longer plateau phase than the base material, and then the stiffness of the structure increases due to compaction. In order to improve the stiffness of the structure and, above all, to be able to control or modify it according to the application, some researchers [50–54] have proposed in recent years different auxetic cell topologies and methods to obtain auxetic structures with variable stiffnesses, being another area that can provide promising results and hence worthy of further research.

In light of the above, and as can be concluded from the reviews on this subject appeared in the last few years [29,55,56], it seems clear that there is a great interest in continue studying auxetic structures to be able to extend their use to different fields. Furthermore, it seems that it will involve the use of additive manufacturing techniques that allow the implementation of cells with complex geometries in order to achieve the required properties for specific applications. This type of study is a challenge since, on the one hand, it is necessary to understand the behaviour of these structures under different types of load and their relationship with the different geometric parameters of the cells and, on the other hand, since they are manufactured using additive technologies, it must be kept in mind that certain variables intrinsic to these manufacturing methods (such as precision or orientation) can also affect the final response of the structure [57–59]. Therefore, it is necessary to carry out more experimental studies to increase knowledge about these structures and the different types of cells that can be proposed so that their use can be extended to more engineering applications.

This work proposes the experimental study of an auxetic structure manufactured by 3D printing (stereolithography additive manufacturing technique) with a polymeric material. In order to achieve the auxetic behaviour in the three directions, a non previously studied re-entrant cell based on cylindrical elements is proposed. The dimensions of the cylindrical elements could help to modify the stiffness structure as required. The work analyses the quasi-static and dynamic behaviour of such a structure. To this end, different experimental tests have been carried out to try to understand the mechanical response of the structure as a function of the type of load, the quantity and size of the unit cells and the applied strain rate. It is considered that the results obtained from the proposed auxetic structure can contribute to the knowledge of both polymeric auxetic structures and the use of additive manufacturing methods for such structures.

2. Manufacture of the auxetic structure

In order to carry out an experimental study on auxetic structures, it is necessary to think about two fundamental things: firstly, which unit cell will be used to develop the structure and secondly, how the structure will be manufactured. The final decision usually depends on both questions. Depending on the cell to be studied (topology, size, etc.), there are manufacturing methods that may be more suitable than others (in terms of precision, materials, cost, etc.) and therefore, depending on the availability of the manufacturing method, certain unit cells can be developed. In this work we have proposed the experimental study of a polymeric auxetic structure composed by a type of re-entrant unit cell that has not been previously studied experimentally. The structure manufacture has been carried out by means of the stereolithography (SLA) additive manufacturing technique.

As it has been previously mentioned, there are studies that have shown the behaviour of auxetic structures with different types of unit cell (re-entrant, arrowhead, chiral), both numerical and experimental, although mostly in the static regime and with metallic structures. The vast diversity in the design of those unit cells opens the door to a new, and sometimes unpredictable, range of mechanical behaviour and deformation patterns and particularities when the samples are tested. There are mixed pros and cons to consider when choosing the design of the unit cell, specially for those experimental samples obtained

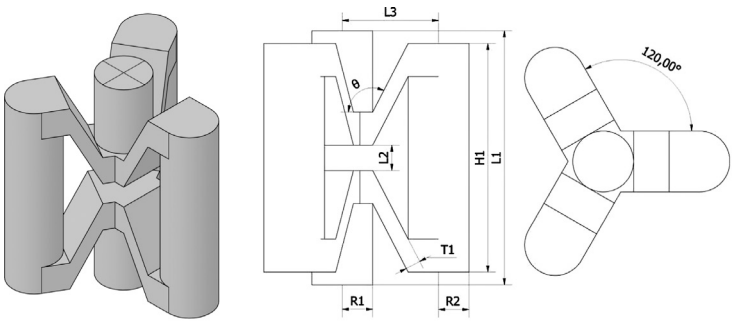

(a) (b)

Parameter	Length [mm]
R1	1.2
R2	1.2
L1	10
L2	1
L3	3.8
H1	9
T1	0.6

(c)

Fig. 1. Re-entrant auxetic unit cell.

by a 3D printing process. Geometrical tolerances and precision detail have to be taken into account depending on the printing technique employed in order to ensure a proper integrity and continuity of the built material, which will diminish the possible particular effects caused by the printing process when tested. In this particular case it has been decided to choose a design based on cylindrical beams, Fig. 1(a).

In Fig. 1(c) the geometrical magnitudes of the unit cell here considered are shown. The unit cell proposed has been chosen due to several reasons: it is a simple and sturdy unit cell to print and therefore it will allow to obtain a less complex structure to study and understand as an initial step. The presence of cylinders whose dimensions can be easily adjusted to modify the stiffness of the structure, has been considered that could be positive for use it in structural elements subjected to impacts. Moreover, it is considered that the chosen unit cell with only three arms can be an appropriate starting point to understand the behaviour of other cells with more arms, which may be more costly to manufacture.

Geometrical parameters taken for the unit cell and shown in Fig. 1(c) were settled considering previous factors such as: a balance between the re-entrant angle (θ) and the room available for movement in the lateral direction, that should be the same in the inner and outer supports of the unit cell as they move in unity. On the other hand, it is pursued to minimize the density as a percentage of the whole lattice taking into account the resolution limitations (minimum printable layer height) of the printing technique so that the final unit cell size does not produce a defective final printed structure.

The additive manufacturing technique used in this work, as it has been already mentioned, is the Stereolithography (SLA). The SLA printing methodology uses a laser source projected over a platform to obtain the desired specimens. This beam of light goes across a liquid tank filled with a polymeric resin with photo-initiators and produces the selective curing in the surface areas hit by the ray trajectory. The curing process is done in the platform plane following a layer-by-layer building where the specimen is sustained by supports that aid the correct growth of the sample and its attachment to the building bed. The resolution of the printing not only comes defined by the laser diameter but also by the increment of the vertical displacement between each layer that can be selected by the user. In stereolithography-based current commercial printers, the aforementioned resolution runs in the range from hundreds of micrometers up to dozens. Once the specimen is printed it must be washed using an Isopropyl alcohol solution for a short period of time described by the provider. After washing the print, and once is properly rinsed, the sample may be cured in a ultraviolet chamber that modifies its mechanical properties by promoting the interaction and the cross-linking of polymer chains. Submitting the specimen to a bath of UV beam-lights during certain time and in a specific temperature, the mechanical properties can increase according to the time exposure until a maximum limit is reached.

This printing technique has been chosen for this work because the specimens to be manufactured will have a higher quality compared with the ones obtained by other methodologies and techniques developed so far, such as FDM. The finest accuracy of the laser enables the design and creation of complex, thin, angled geometries in a versatile and fast way. It is worth to mention that previous studies [60] have proven that sample manufacturing through this technique leads to the obtention of high quality and high repeatability parts with final properties that does not depend on the printing parameters. With this, and once adjusted the geometrical parameters in the cell according to the printer capacity, it can be ensured that the differences found in the mechanical behaviour of the different samples are independent from the way they are obtained. Therefore the mechanical variations that may appear are essentially depending on the lattice stack configuration or testing conditions, among others.

The material chosen to obtain the auxetic structures proposed in this work is a photopolymerizable resin that can be used to manufacture different specimens by stereolithography (SLA) in the non-professional SLA machine *Form 2* from Formlabs®. The resin is called Durable and it is commonly used to prototype parts that would be made from polypropylene (PP). The use of this resin is due to the fact that its mechanical properties [60] seem to be suitable for use in elements that will be subjected to large deformations or impacts, which is one of the potential applications of the proposed auxetic structure.

3. Experimental procedure

Once the unit cell to be used and the manufacturing method chosen have been defined, this section will detail the experimental tests carried out to study the auxetic structure. Quasi-static compression tests and Split Hopkinson Pressure Bar (SHPB) tests have been carried out to analyse the response of the structure in both static and dynamic regimes. The equipment employed as well as the details of the tests carried out and the different specimens used are described below.

3.1. Quasistatic compression

The compression tests were carried out in a universal servo-hydraulic equipment (manufactured by SERVOSIS™) with a 10 kN load cell (ME 401/1 + PCD 1065W). The upper test compression plate has a hinge that avoids any shear loading due to small differences in parallelism between the specimen faces and hence assures a correct performance of the test. The machine plates (tungsten carbide polished plates) that are in contact with the upper and lower faces of the test specimens were lubricated to ensure the correct application of the compression load and to reduce any other loading phenomena that could appear. The servo-hydraulic equipment directly provides force and displacement data. In addition, a camera recorded the whole process of compression of the specimens. The images obtained allow to identify the instants in which certain physical processes occur and hence relate them with the data obtained. All the specimens were tested at a cross head speed of 0.02 mm/s.

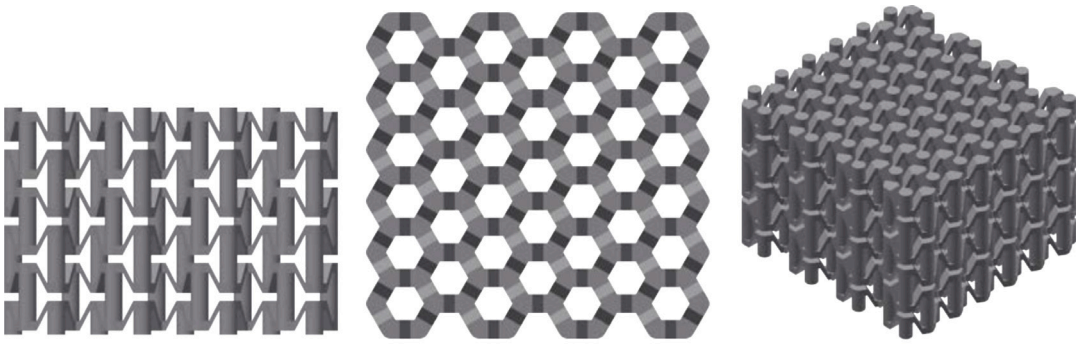

(a) Front view (b) Top view (c) Side view

Fig. 2. Different views of quasi-static test samples with a scale 1.

Table 1
Dimensions and relative density of the different lattices tested under quasi-static loading.

Scale	Cell layers	Length [mm]	Width [mm]	Height [mm]	$\frac{\rho}{\rho_0}$
1.0	3	41.89	44.2	30	0.53
1.0	2	41.89	44.2	20	0.51
1.2	2	42.37	39.36	24	0.53
1.5	2	43.09	49.02	30	0.52

Table 2
Summary of SHPB perfomed tests.

Scale	Cell layers	Heigth [mm]
0.9	4	36
0.9	3	27
0.9	2	18

In order to study the behaviour of the auxetic cell chosen, different auxetic structure specimens were manufactured. The dimensions of the different specimens used for the quasi-static compression tests are shown in Table 1. The last column includes the relative density of the cell with respect to the raw material density ($\frac{\rho}{\rho_0}$), all the cell vary around 50% of the density of the raw polymer. Specimens with different number of cells through the thickness (cell layers) and specimens with the same cell layers but different thickness (modifying the scale) were tested in order to study the influence of both variables (number of cell layers and scale). The specimens were designed in order to be as square as possible (same size in the total length and width) to facilitate the comparison between the different models, therefore the cases with different scales have different number of cells in those directions. Fig. 2 shows as an example three different views of the lattice with a unit cell scale of 1 and three unit cells through the thickness.

3.2. Split Hopkinson Pressure Bar (SHPB)

Dynamic tests were carried out using a SHPB. The SHPB impose a dynamic load on the auxetic sample similar to that at which the structure will be exposed in a dynamic situation and high energy events. As seen in Fig. 3 the SHPB system consists on a 22 mm diameter steel (F114) striker, input and output bars of 500, 2600 and 1500 mm length, respectively. In addition, the system has a gas launcher that, using pressurized air, is able to fire the striker onto the input bar promoting the stress pulse, which travels inside the bar and hits the specimen located between the input and output bar, generating the desired compression. At the interfaces between the loading bars and the specimen, the stress pulse separates into reflected and transmitted pulses at the input and output bars. Part of the pulse is transmitted to the output bar and reflected in the input bar due to the compression and mismatch impedance of the bar and the specimen. At the end of the system there is an anvil that works as a stopping mechanism. The impact velocity of the striker is obtained by means of laser barriers through a velocimeter and it can be modified or adjusted changing the pressure in the gas launcher. The strain induced in the input and output bars were measured using strain gauges in both bars and hence being able to obtain the stress–strain curves on the specimen, using 1D theory. Alignment of the bars was checked prior to testing using the impact velocity and the strain pulse magnitude and comparing the theoretical values. For more information about data reduction method and equilibrium assessment the reader is referred to [61,62]. Since there is not an explicit standard for this type of test procedure nor material, it was decided to follow the recommendations contained in ISO 18872 [63] regarding dynamic characterization of polymers. All dynamic test were recorded by means of a high speed camera (Photron SA-Z) in order to capture the whole process of dynamic compression and hence being able to relate the data obtained with the physical behaviour of the auxetic structure.

The specimens for the dynamic tests were designed taking into account the limitation imposed by the diameter of the SHPB bars. Since the bars have a diameter of 22 mm, the aim was to obtain cylindrical specimens as close as possible to that size. Finally, taking into account the geometry of the unit cell used, it can be considered that the manufactured specimens are quite close to cylindrical with a diameter of 19.93 mm (19.93 mm in the x-axis and 19.26 mm in the y-axis). As in the case of the quasi-static compression tests, specimens with different number of cells along their height (cell layer) were made so that specimens with 2, 3 and 4 layers of cells were printed. Fig. 4 shows as an example a sample with 4 cell layers in height. In order to obtain the specimens with the mentioned dimensions it was necessary to scale the original unit cell size by 0.9, so that each unit cell for dynamic tests were 9 mm tall (z-vertical axis) and represented one layer of the structure; therefore the total height of the samples was 9 mm times the number of cell layers. For each specimen type, 3 tests were carried out at an average speed of 7.73 ± 0.31 m/s, Table 2.

4. Results and discussion

Once the tests carried out and the specimens used in quasi-static and dynamic regimes have been described, this section will show both the results obtained and their analysis. The different specimens used will allow to study how the number of cells along the height of the specimens as well as the scale used in the manufacture of the unit cell can influence the behaviour of the proposed auxetic structure at different strain rate ranges.

4.1. Quasistatic compression

4.1.1. Number of cell layers influence

In order to study the effect of the number of cell layers used through the height, quasi-static compression tests were carried out on specimens with 2 and 3 cell layers.

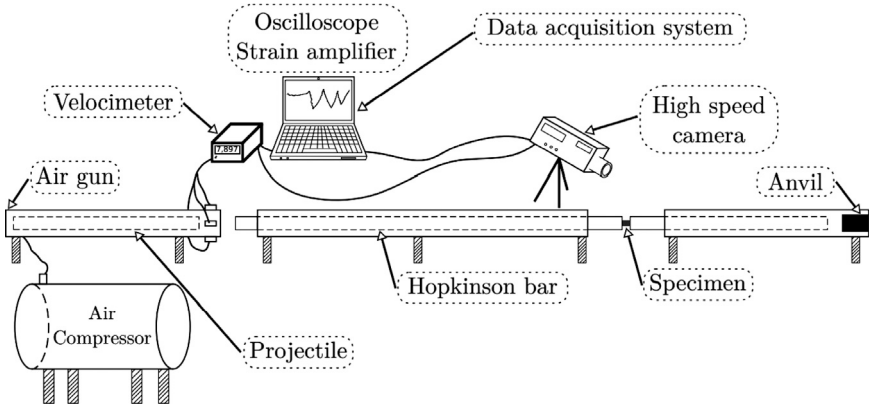

Fig. 3. Configuration of the SHPB tests performed.

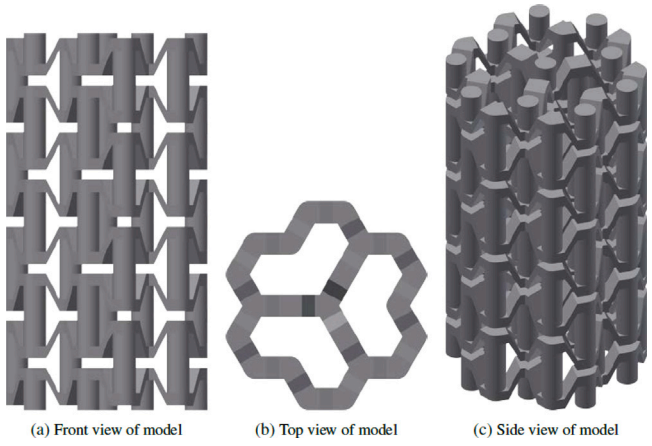

Fig. 4. Example of 4 layered specimen used in SHPB dynamic tests.

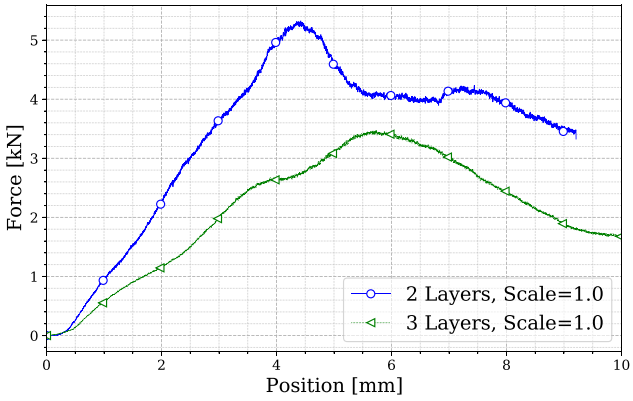

Fig. 5. Force–displacement curves in quasistatic compression tests.

• Different number of cell layers, different height:

First of all, specimens with different numbers of cells along the thickness, and thus different heights, were tested. All other dimensions were kept constant. Fig. 5 shows the force–displacement results provided by the equipment used in the test. In this figure, it can be seen how in both cases the force increases up to a maximum value and then decreases. It is observed that the number of cell layers has a clear influence in the force evolution, as other researchers have reported [64]. The specimen with three layers of cells has a lower peak force than the specimen with only two layers. The differences in both peak force and stiffness are remarkable. To try to understand these results and to see if the slopes between the two cases are really so different, the engineering stress–strain curve (Fig. 6(a)) has been obtained so that the comparison between the two cases is more coherent. In addition, the images obtained during the tests have been analysed in order to be able to relate the different points of the curves with the physical phenomena that are appearing (Figs. 7 and 8). From these images it is possible to measure the Poisson coefficient of the samples during the loading (Fig. 6(b)).

In Fig. 6(a), the first thing that can be observed is that when comparing engineering stress versus strain in both cases, the elastic slopes are very similar until a strain of a little more than 10% is reached in the 3-cell layer case. A 10% strain represents a vertical displacement of 2 and 3 mm in the 2 and 3-cell layer cases, respectively. Due to the geometry of the cells, the cell cylinders have a space of 1 mm to move freely before coming into contact; therefore, 2 and 3 mm is precisely the distance needed in the 2 and 3-cell layer cases for all cell cylinders to be in contact with each other and between the top and bottom plates. Thus, it can be said that both cases have an almost identical initial behaviour until all the cylinders come into contact. From that point on, a different behaviour can be observed between the 2 and 3-cell layer cases. In the 3-cell layer case, there is a slope change that coincides with a slight misalignment displacement between some of the bars that are in contact (Fig. 8(d)). This displacement between the cylinders in the middle layer means that the specimen is not able to withstand much more force and the maximum engineering stress is reached. As the lateral displacement increases, the stress decreases.

In the case of 2 layers of cells, it is observed that once all the cylinders come into contact, the engineering stress continues to increase linearly until it reaches the maximum. In this case, it is observed that before reaching the maximum, a slight misalignment appears between some cylinders, as in the previous case (Fig. 7(c)). In this case, as there is no intermediate cell layer, the displacement is not so large and hence the specimen is able to withstand greater forces. Once the maximum value is reached, the misalignment increases so that appears some interpenetration between the two layers of cells that makes the stress decrease and the specimen tends to be completely crushed (Fig. 7(e)).

The results obtained show that having more number of cells through the height seems to promote the lateral displacement of the structure and makes it more unstable, so that the maximum stress values are lower and are given for a smaller strain. In the case of considering the use of this type of structure for an energy absorption application, it is necessary to take into account that the area under the stress–strain curve in Fig. 6(a) is the energy density (J/m^3). It can be seen that before the contact of the cylinders ($0 \leq \varepsilon \leq 0.1$) both structures are capable of absorbing the same amount of energy. Once the cylinders come into contact $\varepsilon \geq 0.1$, it is clear that having more layers of cells would be less efficient.

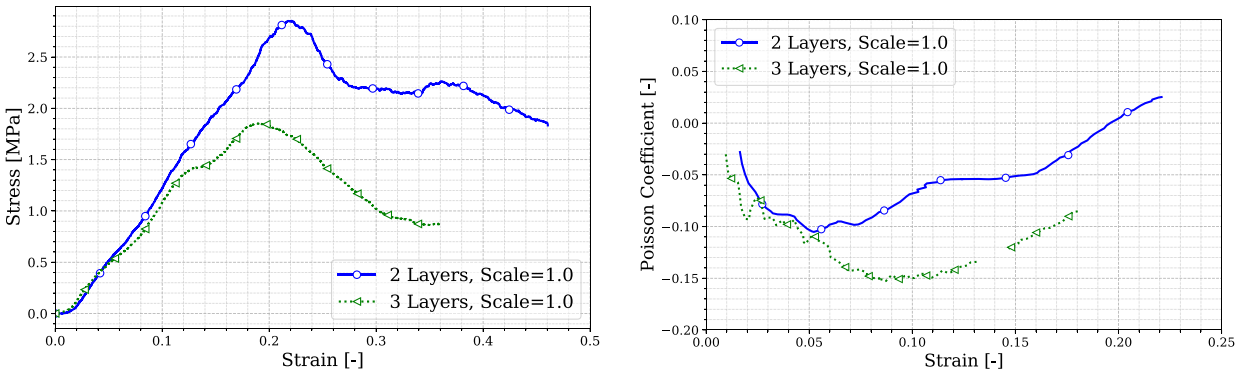

(a) Engineering stress-strain curves (b) Poisson coefficient

Fig. 6. Experimental results from quasistatic compression tests for specimens with different number of cell layers.

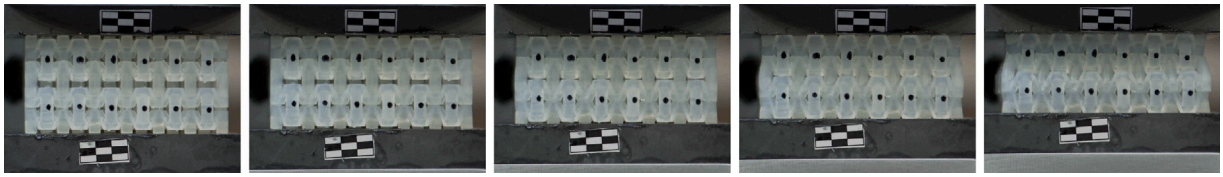

(a) $\varepsilon = 0.0$ (b) $\varepsilon = 0.05$ (c) $\varepsilon = 0.105$ (d) $\varepsilon = 0.155$ (e) $\varepsilon = 0.215$

Fig. 7. Deformation frames for specimen with 2 layers and scale = 1.0.

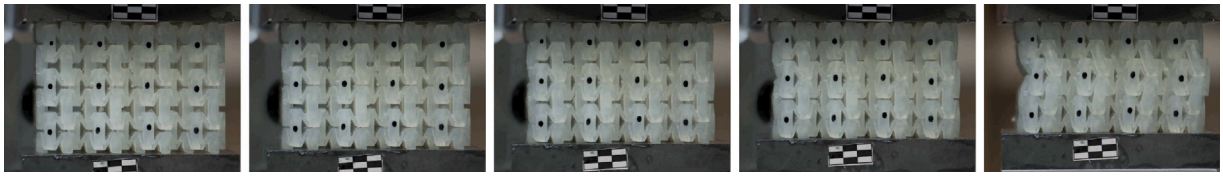

(a) $\varepsilon = 0.0$ (b) $\varepsilon = 0.03$ (c) $\varepsilon = 0.08$ (d) $\varepsilon = 0.117$ (e) $\varepsilon = 0.16$

Fig. 8. Deformation frames for specimen with 3 layers and scale = 1.0.

Fig. 6(b) shows the evolution of the Poisson's ratio as the strain increases in the specimens. It was measured until a strain value around which large displacements and interpenetration of cell bars appeared (18%–20%), leading to invalid measurements. It is observed that the value of the Poisson's ratio is negative until approximately the strain in which the maximum peak force is reached, as it was expected for the proposed auxetic structure. Similar trends and values have been measured for all samples analysed.

- Different number of cell layers, same height:

In view of the above results, it would be reasonable to try to determine whether the observed behaviour is due to the high number of cell layers or to the higher height of the specimen, making it more unstable in those cases. Therefore, two specimens with the same height (30 mm) and different number of cell layers (3 and 2) have been tested. In order to obtain a specimen with the same height (30 mm) but only two cell layers a scale of 1.5 was applied to the original cell. Thus, the specimen with 2 layers of cells has longer rods and a larger diameter than the specimen with 3 layers of cells (with the original cell) (Table 1). Due to the accuracy limitations of the desktop SLA equipment used it was not possible to test a structure with 4 layers and a height of 30 mm.

Fig. 9(a) shows the engineering stress versus strain curves for the cases studied. It can be seen that the maximum stress is reached for the case of two layers of cells, like in the previous section. Similarly, it can be seen that the curves are similar until approximately a 10% strain is reached, point at which all the bars come into contact with each other. It can be said that this first slope corresponds to the initial auxetic behaviour of the structure, previous to the contact of the bars; during this slope the load path is controlled by the arms of the cell (Fig. 10(a)) and hence a gentler slope is obtained. The case with 3 layers of cells is the same as the one analysed in the previous section. However, in the case with two layers of cells, some differences can be observed with respect to the 2-cell layer case analysed above. In this case, it can be seen that there is a slight tilting of the bars when they all come into contact (Fig. 11). This may be due to the fact that in this case the bars are longer and induce that inclination, which goes against a stable equilibrium. However, there is also a change of slope with a sharp increase in the value of the stress. This may be due to the fact that the diameter of the bars in these cases is greater (scale 1.5) than in the previous ones (scale 1.0). This fact could compensate the inclination of the bars with a more stable contact between the bars and therefore increasing the force that they can withstand. In this case the load path pass through the contact between the cylinders (Fig. 10(b)) producing a stepper slope or stiffness of the structure than the obtained when the arms of the cell control the load path (Fig. 10(a)). The cell with 2 and 3 cells and scale 1.0 does not have enough stable contact area between the cylinders promoting a unstable premature buckling. Therefore higher contact area or more stable contact is required to achieve this double step behaviour. In order to analyse the evolution of the energy density for the different specimens during compression, Fig. 9(b) is shown. It can be seen how both trends are similar up to point A ($\varepsilon = 10\%$), point of contact between the cylinders. Beyond this point it is clear that, even further from the maximum stress (Point B),

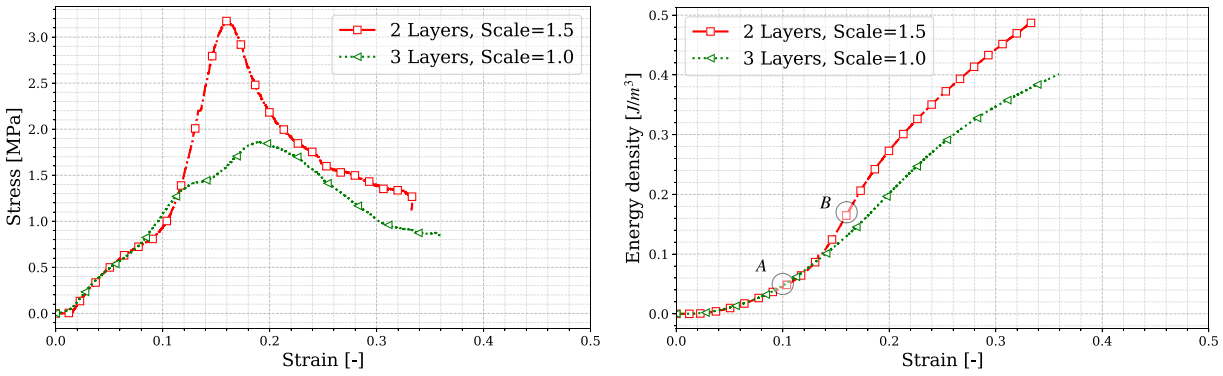

(a) Stress strain curve (b) Energy density evolution

Fig. 9. Experimental curves from quasistatic compression tests for specimens with different cell layers and same height.

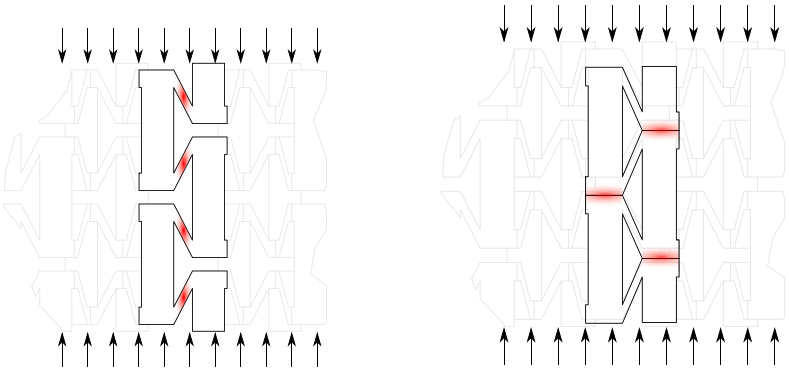

(a) Cell arms dominated (b) Cylinder contact dominated

Fig. 10. Schematic representation of the cut-off of the cells at different stages during deformation.

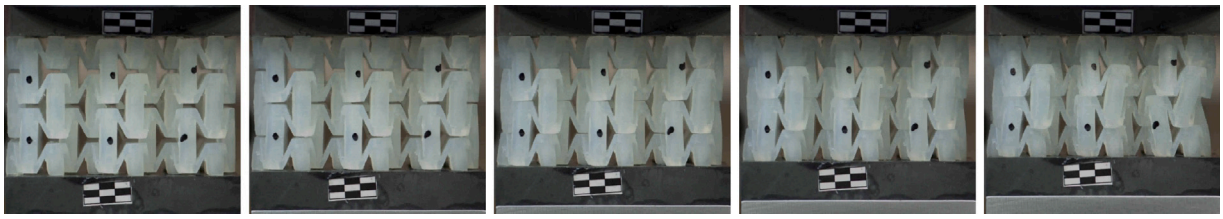

(a) $\varepsilon = 0.0$ (b) $\varepsilon = 0.033$ (c) $\varepsilon = 0.067$ (d) $\varepsilon = 0.100$ (e) $\varepsilon = 0.133$

Fig. 11. Deformation frames for specimen with 2 layers and scale = 1.5.

the stability of the 2 layer specimen produces a higher energy density absorption.

Analysing in depth the energy density absorbed by the samples during the compression

This is an interesting behaviour because it shows that modifying the dimensions of the bars of the cells (mainly the diameter or the contact geometry), the stiffness of the structure can be controlled or modified. Once the bars get in touch it appears a second slope, which is around 4,5 times higher than the first one ($\frac{1}{0,1}$ vs. $\frac{2,25}{0,05}$). Therefore the unit cell proposed could be used to design a tunable stiffness structure. Although the stiffness of the lattice is low in both cases (with respect to the raw polymer [60]) it is in the range of other cells proposed by other authors, such as Chen and Fu [54]. This low stiffness promotes soft behaviour in case of compression, reducing the deceleration suffered by the surrounding structures. The difference with the cell proposed by Chen and Fu is the relative density (Table 1); the proposed cell presents an order of magnitude more than other cells. This characteristic could be interesting in case of dynamic events in which the inertia play a major role.

Another difference of this case with respect to the previous 2-cell case (with scale 1.0) is regarding to the stress reduction once the maximum stress is reached. In this case it can be observed that the ongoing lateral displacement causes an overlapping and interpenetration between the bars of the two layers of cells that causes the stress to decrease more than in the previous case, without reaching a constant value.

As it was observed in the previous section, the results obtained show that a specimen with more number of cells through the height (for the same height) leads to smaller stress values, although specimens with more cell layers would be desirable to observe a clear trend. This behaviour seem to be related to the stability of the structure and how it evolves under compression, so that a higher peak stress at a lower strain is obtained in the case with higher scale (bigger cylinders). To try to clarify this phenomenon, the scale variable will be studied.

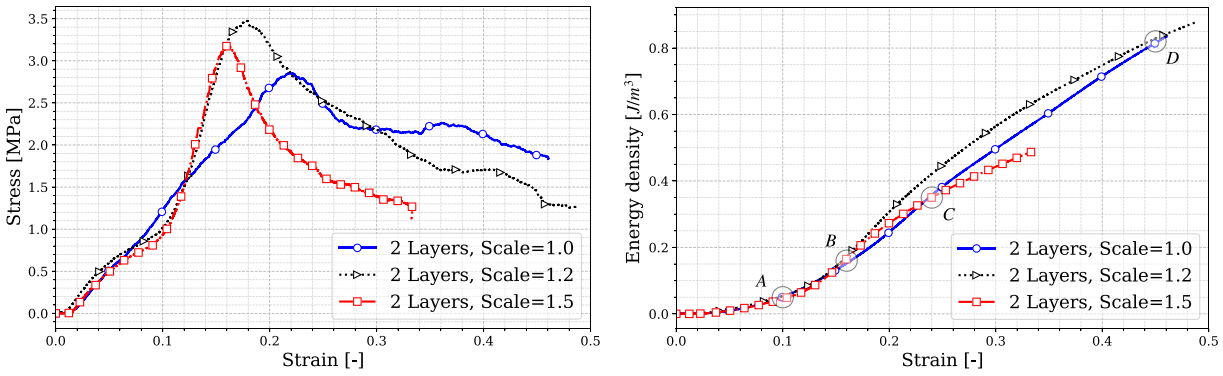

(a) Stress strain curve (b) Energy density evolution

Fig. 12. Experimental results from quasistatic compression tests for specimens with different scales.

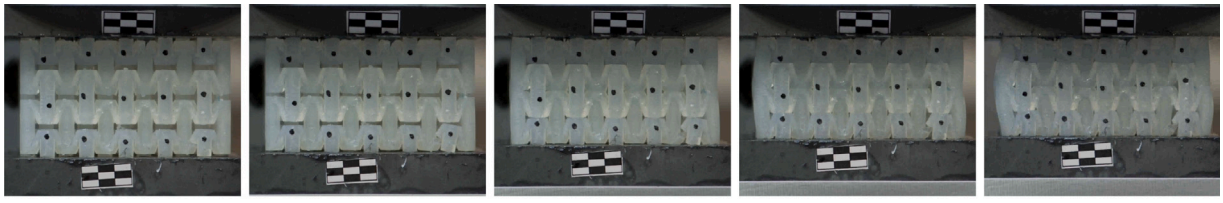

(a) $\varepsilon = 0.0$ (b) $\varepsilon = 0.04$ (c) $\varepsilon = 0.108$ (d) $\varepsilon = 0.154$ (e) $\varepsilon = 0.179$

Fig. 13. Deformation frames for specimen with 2 layers and scale = 1.2.

4.1.2. Scale/height influence

In the previous section, in order to study the influence of the number of cell layers considering the same height, the cell scale variable was introduced. In this section we have considered the study of the influence of this variable by comparing the results of specimens with the same number of cell layers (2) but with different scale (scale 1, 1.2 and 1.5) so that the height between the different specimens is different (Table 1).

Fig. 12(a) shows the engineering stress versus strain results of specimens with the same number of cell layers and different scale. It can be seen that in all three cases a similar behaviour is observed until approximately a 10% strain is reached. Around this point, as mentioned above, the complete contact between the different cylinders of the specimens occurs. Once this point is reached, differences are observed between the case with scale 1 and the cases with scale 1.2 and 1.5. Fig. 12(b) shows the evolution of the energy density, again the trend of the different specimens is similar up to the point A (ε = 10%), point of contact between the cylinders, no matter the scale it is. Beyond this point the higher the scale is, the more stable the contact is (Fig. 10(b)) and hence more energy is absorbed. Once the maximum stress is reached (point B) the stability controlled by the slenderness of the cylinders controls the unloading and the trends change, as it will be explained later. Depending on the amount of the strain reached, the energy of the specimen with scale 1 could be more efficient in terms of energy density (point *C* and *D*).

In the case with scale 1, as already mentioned, it can be seen that the engineering stress increases linearly until it reaches the maximum. Before reaching this maximum, a slight misalignment appears between some cylinders. Once the maximum is reached this misalignment increases so that interpenetration appears between the two layers of cells. This fact causes the engineering stress to decrease and the complete crushing of the specimen. The cases with scale 1.2 and 1.5 show a very similar change of slope after reaching 10% strain. This change in slope is probably due to the increase in the dimensions of the bars with respect to the case of scale 1. As it has been seen in the previous section, a higher scale (bigger rods) promotes an increase in stiffness and a higher maximum stress because of a better stability. However, it is observed that the difference in the maximum stress value for the cases of bigger scales are small and not very representative. Even so, some differences can be seen between the scales 1.5 and 1.2 regarding the stress reduction once the maximum stress is reached. The case with a scale 1.5 shows a faster decrease in stress than in the case with scale 1.2. This could be related to the different evolution of the bars observed during the compression process. It can be seen that the case with scale 1.5 presents an earlier and more noticeable tilt and displacement of the bars, probably due to its larger dimensions, that trigger the faster decrease of the stress. The case with scale 1.2 shows a slight interpenetration between the bars, but also a similar displacement or buckling to that observed in the case of scale 1 (Fig. 13). This makes that the decreasing of the stress in the case with scale 1.2 is in between the other two scales. These differences are caused by the difference in length and diameter of the bars between the studied specimens. Therefore, the interpenetration between cells is favoured in the cases with bigger cells, leading to a fast decrease of stress. Whereas the displacement between the bars or buckling is favoured in the cases with smaller cells.

4.2. Dynamic tests (Split Hopkinson Pressure Bar)

The results obtained in the dynamic tests carried out on the SPHB for the different cases studied are shown below. The effect of the number of cell layers in the specimens when they are subjected to a dynamic load has been studied. The specimen data and test velocity are given in Section 3.2.

Fig. 14 shows the engineering stress–strain curves for the three cases studied. The figure shows that for each case, different number of rising slopes and plateaus can be distinguished, depending on the number of cell layers. The fewer the number of cell layers, the higher the number of rise slopes and plateaus. This is associated with the duration of the incident pulse and the effect that it has on the specimen. In order to relate the results obtained to the physical phenomena that occurs in the specimen, the images obtained during the tests are analysed. Fig. 15 shows a series of images of the specimen with 2 cell layers during the generated pulse. When the pulse arrives, the first layer of cells begins to

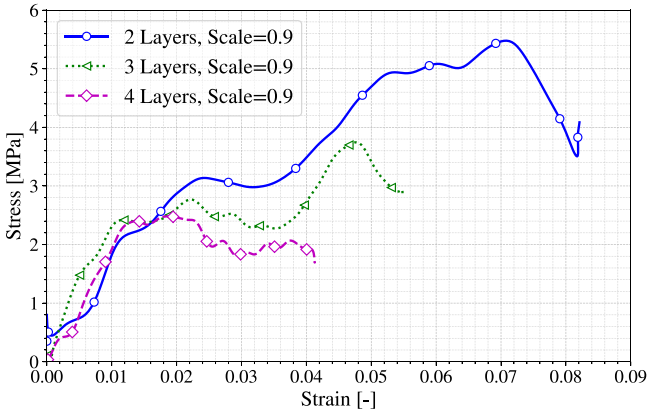

Fig. 14. Stress strain curves in SHPB tests.

move to the right (Fig. 15, $\varepsilon = 0$) increasing the stress in the specimen, which matches with the first slope that can be seen in Fig. 14. When the strain $\varepsilon = 0.022$ is reached, the movement of the first layer of cells finishes, and thus the increase in stress. In Fig. 15, red circles have been used to mark the spaces between the cylinders so that the difference between the frames can be seen. At the end of the first displacement of the first layer of cells, it can be observed how second layer begins to move (Fig. 15, $\varepsilon = 0.022$). The displacement of the second layer finishes approximately when the value of the strain is $\varepsilon = 0.039$ and there is a certain relaxation in the specimen as this displacement has not caused an increase in stress, Fig. 14 (from $\varepsilon = 0.022$ to $\varepsilon = 0.039$). At $\varepsilon = 0.039$ it can be seen how the first layer of cells is displaced again, (Fig. 15, $\varepsilon = 0.039$) until it reaches a strain $\varepsilon = 0.055$. During this second displacement of the first layer (from $\varepsilon = 0.039$ to $\varepsilon = 0.055$) there is an increase in stress, Fig. 14. From $\varepsilon = 0.055$ up to $\varepsilon = 0.073$, a final displacement of the second layer and the first layer of cells is observed again until the maximum stress value is reached, Fig. 14. In Fig. 15 ($\varepsilon = 0.073$) it can be seen that the gaps between the layers of cells are barely observed and that the whole specimen is in contact with the surface on the left.

The images of the test corresponding to the structure with 3 cell layers, Fig. 16, show a similar behaviour to what it was described above. The first layer of cells starts to move and the first slope appears in Fig. 14. When a strain of approximately $\varepsilon = 0.011$ is reached, the second layer of cells starts to move, followed by the displacement of the third layer until a strain of $\varepsilon = 0.037$ is reached with barely any increase in stress. Then the first layer of cells begins to move again (at $\varepsilon = 0.037$), increasing the slope until the maximum stress is reached. At this point, the pulse generated ends. In this case it can be seen that for the maximum strain reached there are still some gaps between some of the cylinders of the cells, so that a complete compression of the structure has not been achieved.

Fig. 17 shows the images obtained during the 4-cell layer case test. As in the previous cases, it can be seen that the first layer of cells starts to move until reaching a strain $\varepsilon = 0.011$, causing the first slope in the engineering stress–strain curve of Fig. 14. At $\varepsilon = 0.011$ begins the displacement of the second, third and fourth layer of cells in a chained way. When reaching a strain of approximately $\varepsilon = 0.023$, the fourth layer of cells finishes its displacement and then some movement of the third and second layers can be seen, generating a slight decrease in the stress registered. Finally, the specimen reaches its final strain without any further displacement of the first layer of cells nor an slope increasing in stress.

The results show a clear influence of the number of cell layers in the mechanical behaviour observed. It can be said that the increasing in stress is related to the displacement or compression experienced by the first layer of cells, as it is depicted in the first idealized slope (A–B) in Fig. 18. This cell layer is the one in the side of the movement of the bars. Once this occurs, there is a series of chained displacements of the following cell layers so that the strain increases, but not the stress measured (Plateau B–C). The stress value reached in the first increment is approximately the same in all cases, which is reasonable, since this increment is related to the same physical phenomenon (displacement of the first layer of cells). The second stress increase observed in the 2 and 3-cell layer cases (related to the second displacement of the first layer of cells) is similar, although in the case of 3 cell layers it is smaller (slopes C–D and C–D' in Fig. 18). This may be due, to the fact that in the 3 cell layer case there are two layers of cells that have been displaced, instead of only one as happened for the 2 cell layer case. Therefore the differences observed regarding the stress reached could be related to an inertial effect due to the mass that the cell layer has in front of it. Therefore when the cell has more number of cells in front of it reaches a smaller stress. Since the pulse duration in all cases is the same (and hence the maximum displacement imposed), in the 2 layer case the first layer can be displaced several times. Nevertheless in the 4 cell layer case, the first layer cannot be displaced more than once, showing only one rising slope and one plateau. In view of the images obtained in all the cases it can be said that the complete compression of the specimens is not reached, as the gaps between cells are not completely covered. This behaviour is also affected by the mass or inertia of the cell. The relative density of the cell around 0.5, Table 1, confers to the lattice structure a behaviour that could be useful to use the structure as an isolator for dynamic events.

In terms of energy absorption by the structures, similar trend to what is observed in quasistatic tests can be seen during the first slope. The amount of energy density is approximately the same for all cases until the first cell layer comes into contact with the following cell layer. After that instant, it can be observed that the energy density depends on the number of cell layers. However, given that the pulse duration and impact velocity are the same in all the cases, the energy imposed in all the tests is the same but the amount of strain reached is different. So, the amount of energy density absorbed per time (J/m^3 s) is controlled by the number of cells: as the number of cells increases the energy absorption per time diminishes. According to what is observed, it is expected that for dynamic events with shorter pulse duration, lower number of cell layers increases the energy absorption of the structure. Whereas, for events with longer pulse time duration, increasing the number of cell layers raises the energy absorption capability. This should be taken into account when designing possible applications for protective structures.

5. Conclusions

In the present work, the experimental study of an auxetic polymeric structure obtained by SLA 3D printing has been carried out. The use of a non previously studied cell design has been proposed and the feasibility of manufacturing this type of structures by means of an additive manufacturing desktop equipment has been shown. Its behaviour under both static and dynamic loads has been analysed. For this purpose, different tests have been carried out to study the influence of different variables such as the number and size (scale) of cells used in the response of the structure at different strain rates.

- In quasi-static regime, the proposed structures behave similarly until the cylinders come into contact. Therefore the free distance between the cylinders could be designed to adapt it to the needs of different applications by varying the initial stiffness of the structure.
- The smallest maximum stresses occurs in cases with more number of cell layers along the thickness due to the instability produced by the displacement of the intermediate cell layer. This instability is due to the number of cells and not so much to the height, as cases with the same height and a lower number of cells do not experience this instability.

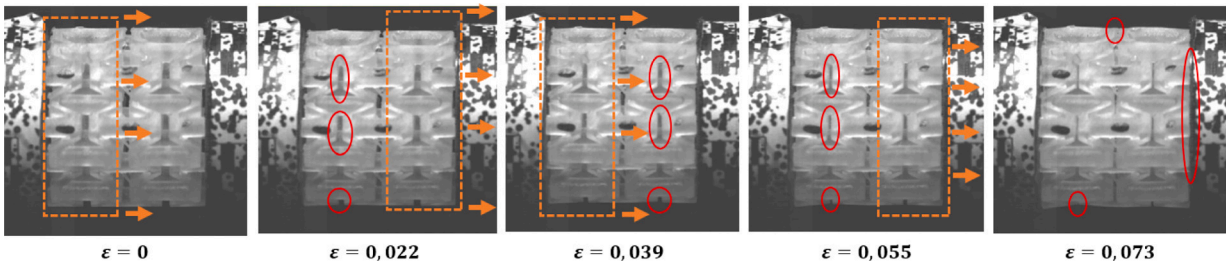

Fig. 15. Images of the 2-cell layers SHPB test.

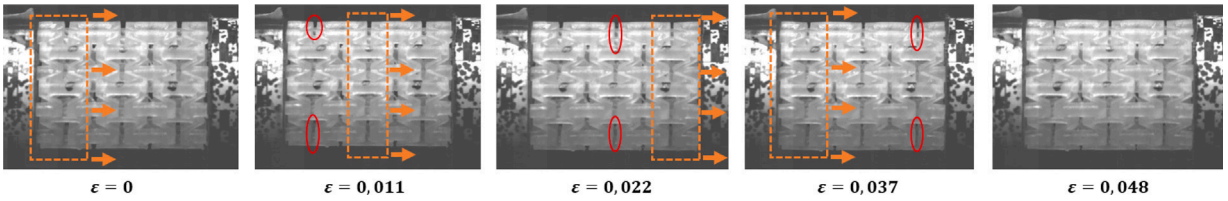

Fig. 16. Images of the 3-cell layers SHPB test.

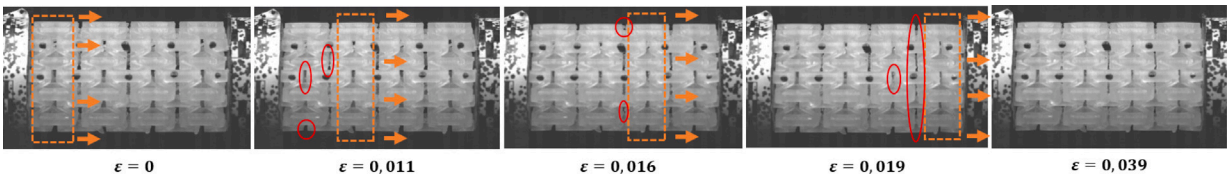

Fig. 17. Images of the 4-cell layers SHPB test.

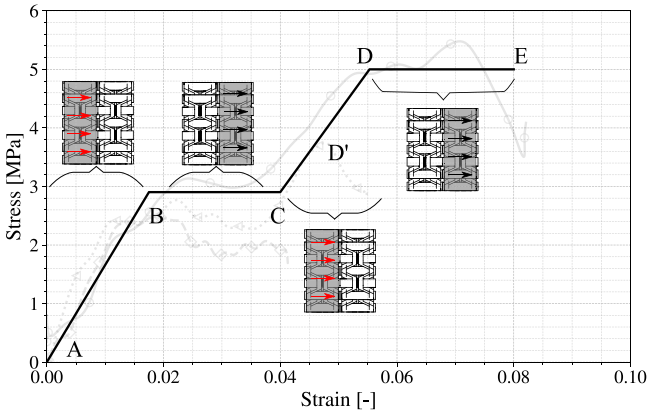

Fig. 18. Idealized specimen behaviour during dynamic compression.

- For the same number of cell layers, a larger cell scale promotes higher maximum stress values due to a higher stability produced by the larger contact area between the cylinders. However, the longer length of the cylinders causes a rapid decrease in stress and instability due to interpenetration between cells.
- According to the results obtained, it can be concluded that it is important to take into account both the number of cells and their size for optimal use of this type of structure. In addition, more stable contact between cylinders, as conical shape, could be implemented improving the stability of the lattice.
- The number of cell layers influences the dynamic behaviour of the proposed structures. Cases with less number of cell layers reach higher stress values due to the fact that the compression pulse is able to generate a higher displacement of the cells and therefore a higher compression in the cases with less number of cells.
- It has been observed that the energy density depends on the number of cell layers, which should be taken into account to design potential protective structures under different dynamic loads.
- The tests carried out have allowed to understand the sequence of physical phenomena that appear at high strain rates and how they affect the strain values obtained, but it would be necessary to be able to obtain final values of the complete compression of the structures. Therefore it is necessary to use a SHPB equipment capable of generating a longer pulse duration, since in none of the cases studied it was possible to cover the free space between all the cylinders.

The results and conclusions obtained can contribute to widen the knowledge of auxetic polymeric structures so that designers can take into account the variables that affect them in different load cases and how they can optimize them to achieve optimal behaviour for a given application.

CRediT authorship contribution statement

D. Varas: Conceptualization, Methodology, Data curation, Writing – original draft. **J. Pernas-Sánchez:** Data curation, Writing – original draft, Experimental testing. **N. Fjeldberg:** Specimen design, Experimental testing. **J. Martín-Montal:** Specimen manufacturing, Experimental testing.

Declaration of competing interest

The authors declare that they have no known competing financial interests or personal relationships that could have appeared to influence the work reported in this paper.

Data availability

Data will be made available on request.

Acknowledgements

This research was funded by Ministerio de Asuntos Económicos y Transformación Digital, Gobierno de España grant number DPI2017-85073-R, and Vicerrectorado de Política Científica UC3M (Projects 2013/00413/003 and 2014/00006/003).

References

[1] R.S. Lakes, Foam structures with a negative Poisson's ratio, Science 235 (4792) (1987) 1038–1040, http://dx.doi.org/10.1126/science.235.4792.1038.
[2] F. Scarpa, P.J. Tomlin, On the transverse shear modulus of negative Poisson's ratio honeycomb structures, Fatigue Fract. Eng. Mater. Struct. 23 (8) (2000) 717–720, http://dx.doi.org/10.1046/j.1460-2695.2000.00278.x.
[3] R.S. Lakes, Design considerations for materials with negative Poisson's ratios, J. Mech. Des. 115 (4) (1993) 696–700, http://dx.doi.org/10.1115/1.2919256.
[4] M. Bianchi, F. Scarpa, C. Smith, Stiffness and energy dissipation in polyurethane auxetic foams, J. Mater. Sci. 43 (17) (2008) 5851–5860, http://dx.doi.org/10.1007/s10853-008-2841-5.
[5] A. Bezazi, F. Scarpa, Mechanical behaviour of conventional and negative Poisson's ratio thermoplastic polyurethane foams under compressive cyclic loading, Int. J. Fatigue 29 (5) (2007) 922–930, http://dx.doi.org/10.1016/j.ijfatigue.2006.07.015.
[6] F. Scarpa, P. Pastorino, A. Garelli, S. Patsias, M. Ruzzene, Auxetic compliant flexible PU foams: static and dynamic properties, Phys. Status Solidi B 242 (2005).
[7] F. Scarpa, Auxetic materials for bioprostheses, IEEE Signal Process. Mag. 25 (5) (2008) 125–126.
[8] J.B. Choi, R.S. Lakes, Design of a fastener based on negative Poisson's ratio foam, Cell. Polym. 10 (3) (1991) 205–212.
[9] F. Scarpa, J. Giacomin, Y. Zhang, P. Pastorino, Mechanical performance of auxetic polyurethane foam for antivibration glove applications, Cell. Polym. 24 (5) (2005) 253–268, http://dx.doi.org/10.1177/026248930502400501.
[10] D. Ieşan, Pressure vessel problem for chiral elastic tubes, Internat. J. Engrg. Sci. 49 (5) (2011) 411–419, http://dx.doi.org/10.1016/j.ijengsci.2011.01.003.
[11] M.N. Ali, J.J.C. Busfield, I.U. Rehman, Auxetic oesophageal stents: structure and mechanical properties, J. Mater. Sci., Mater. Med. 25 (2) (2014) 527–553, http://dx.doi.org/10.1007/s10856-013-5067-2.
[12] A.E.H. Love, A Treatise on the Mathematical Theory of Elasticity, fourth ed., Dover Books on Advanced Mathematics, Dover, New York, 1944.
[13] J. Vincent, Structural Biomaterials, third ed., Princeton University Press, 2012.
[14] K. Evans, Auxetic polymers: a new range of materials, Endeavour 15 (4) (1991) 170–174.
[15] Y. Li, C. Zeng, On the successful fabrication of auxetic polyurethane foams: Materials requirement, processing strategy and conversion mechanism, Polymer 87 (C) (2016) 98–107, http://dx.doi.org/10.1016/j.polymer.2016.01.076.
[16] L. Yang, O. Harrysson, H. West, D. Cormier, Mechanical properties of 3D re-entrant honeycomb auxetic structures realized via additive manufacturing, Int. J. Solids Struct. 69–70 (2015) 475–490, http://dx.doi.org/10.1016/j.ijsolstr.2015.05.005.
[17] L. Gibson, M. Ashby, Cellular Solids: Structure and Properties, in: Cambridge Solid State Science Series, Cambridge University Press, 1997.
[18] L. Yang, O.L.A. Harrysson, H.A. West, D. Cormier, Modeling of uniaxial compression in a 3D periodic re-entrant lattice structure, J. Mater. Sci. 48 (2012) 1413–1422.
[19] I. Masters, K. Evans, Models for the elastic deformation of honeycombs, Compos. Struct. 35 (4) (1996) 403–422, http://dx.doi.org/10.1016/S0263-8223(96)00054-2.
[20] I. Berinskii, Elastic networks to model auxetic properties of cellular materials, Int. J. Mech. Sci. 115–116 (2016) 481–488, http://dx.doi.org/10.1016/j.ijmecsci.2016.07.038.
[21] R. Almgren, An isotropic three-dimensional structure with Poisson's ratio=-1, J. Elasticity 15 (1985) 427–430.
[22] D. Li, J. Ma, L. Dong, R.S. Lakes, Three-dimensional stiff cellular structures with negative Poisson's ratio, Phys. Status Solidi B 254 (12) (2017) 1600785, http://dx.doi.org/10.1002/pssb.201600785.
[23] J. Huang, Q. Zhang, F. Scarpa, Y. Liu, J. Leng, In-plane elasticity of a novel auxetic honeycomb design, Composites B 110 (2017) 72–82, http://dx.doi.org/10.1016/j.compositesb.2016.11.011.
[24] S.H. Chan, M. E. Plesha, R. Lakes, Chiral three-dimensional lattices with tunable Poisson's ratio, Smart Mater. Struct. 25 (5) (2016) 054005, http://dx.doi.org/10.1088/0964-1726/25/5/054005.
[25] X. chun Zhang, H. min Ding, L. qiang An, X. lei Wang, Numerical investigation on dynamic crushing behavior of auxetic honeycombs with various cell-wall angles, Adv. Mech. Eng. 7 (2) (2015) 679678, http://dx.doi.org/10.1155/2014/679678.
[26] P. Zhang, Z. Wang, L. Zhao, Dynamic crushing behavior of open-cell aluminum foam with negative Poisson's ratio, Appl. Phys. A 123 (5) (2017) 321, http://dx.doi.org/10.1007/s00339-017-0757-0.
[27] D. Li, J. Yin, L. Dong, R.S. Lakes, Numerical analysis on mechanical behaviors of hierarchical cellular structures with negative Poisson's ratio, Smart Mater. Struct. 26 (2) (2016) 025014, http://dx.doi.org/10.1088/1361-665x/26/2/025014.
[28] H. Tankasala, V. Deshpande, N. Fleck, Tensile response of elastoplastic lattices at finite strain, J. Mech. Phys. Solids 109 (2017) 307–330, http://dx.doi.org/10.1016/j.jmps.2017.02.002.
[29] J. Zhang, G. Lu, Z. You, Large deformation and energy absorption of additively manufactured auxetic materials and structures: A review, Composites B 201 (2020) 108340, http://dx.doi.org/10.1016/j.compositesb.2020.108340.
[30] E. Friis, R. Lakes, J. Park, Negative Poisson's ratio polymeric and metallic foams, J. Mater. Sci. 23 (12) (1988) 4406–4414, http://dx.doi.org/10.1007/BF00551939.
[31] N. Chan, K. Evans, Mechanical properties of conventional and auxetic foams. Part I: Compression and tension, J. Cell. Plast. 35 (2) (1999) 130–165, http://dx.doi.org/10.1177/0021955X9903500204.
[32] O. Duncan, L. Foster, T. Senior, A. Alderson, T. Allen, Quasi-static characterisation and impact testing of auxetic foam for sports safety applications, Smart Mater. Struct. 25 (5) (2016) 054014, http://dx.doi.org/10.1088/0964-1726/25/5/054014.
[33] N. Chan, K. Evans, Mechanical properties of conventional and auxetic foams. Part II: Shear, J. Cell. Plast. 35 (2) (1999) 166–183, http://dx.doi.org/10.1177/0021955X9903500205.
[34] N. Chan, K. Evans, Indentation resilience of conventional and auxetic foams, J. Cell. Plast. 34 (3) (1998) 231–260, http://dx.doi.org/10.1177/0021955X9803400304.
[35] N. Novak, M. Vesenjak, L. Krstulović-Opara, Z. Ren, Mechanical characterisation of auxetic cellular structures built from inverted tetrapods, Compos. Struct. 196 (2018) 96–107, http://dx.doi.org/10.1016/j.compstruct.2018.05.024.
[36] F. Scarpa, L. Ciffo, J. Yates, Dynamic properties of high structural integrity auxetic open cell foam, Smart Mater. Struct. 13 (1) (2003) 49.
[37] T.C. Lim, A. Alderson, K.L. Alderson, Experimental studies on the impact properties of auxetic materials, Phys. Status Solidi B 251 (2) (2014) 307–313, http://dx.doi.org/10.1002/pssb.201384249.
[38] N. Novak, K. Hokamoto, M. Vesenjak, Z. Ren, Mechanical behaviour of auxetic cellular structures built from inverted tetrapods at high strain rates, Int. J. Impact Eng. 122 (2018) 83–90, http://dx.doi.org/10.1016/j.ijimpeng.2018.08.001.
[39] O. Duncan, L. Foster, T. Senior, T. Allen, A. Alderson, A comparison of novel and conventional fabrication methods for auxetic foams for sports safety applications, Procedia Eng. 147 (2016) 384–389, http://dx.doi.org/10.1016/j.proeng.2016.06.323.
[40] T. Fíla, P. Zlámal, O. Jirousek, J. Falta, P. Koudelka, D. Kytýr, T. Doktor, J. Valach, Impact testing of polymer-filled auxetics using Split Hopkinson Pressure Bar, Adv. Eng. Mater. 19 (10) (2017) 1700076, http://dx.doi.org/10.1002/adem.201700076.
[41] T. Bückmann, N. Stenger, M. Kadic, J. Kaschke, A. Frölich, T. Kennerknecht, C. Eberl, M. Thiel, M. Wegener, Tailored 3D mechanical metamaterials made by dip-in direct-laser-writing optical lithography, Adv. Mater. 24 (20) (2012) 2710–2714, http://dx.doi.org/10.1002/adma.201200584.
[42] C. Qi, F. Jiang, A. Remennikov, L.-Z. Pei, J. Liu, J.-S. Wang, X.-W. Liao, S. Yang, Quasi-static crushing behavior of novel re-entrant circular auxetic honeycombs, Composites B 197 (2020) 108117, http://dx.doi.org/10.1016/j.compositesb.2020.108117.
[43] T.-C. Lim, A 3D auxetic material based on intersecting double arrowheads, Phys. Status Solidi B 253 (7) (2016) 1252–1260.
[44] L. Gu, Q. Xu, D. Zheng, H. Zou, Z. Liu, Z. Du, Analysis of the mechanical properties of double arrowhead auxetic metamaterials under tension, Text. Res. J. 90 (21–22) (2020) 2411–2427, http://dx.doi.org/10.1177/0040517520924850.
[45] D. Prall, R. Lakes, Properties of a chiral honeycomb with a poisson's ratio of — 1, Int. J. Mech. Sci. 39 (3) (1997) 305–314, http://dx.doi.org/10.1016/S0020-7403(96)00025-2.
[46] L. Cabras, M. Brun, A class of auxetic three-dimensional lattices, J. Mech. Phys. Solids 91 (2016) 56–72.
[47] L. Yang, O. Harrysson, H. West, D. Cormier, Compressive properties of Ti–6Al–4V auxetic mesh structures made by electron beam melting, Acta Mater. 60 (8) (2012) 3370–3379, http://dx.doi.org/10.1016/j.actamat.2012.03.015.
[48] Q. Gao, W.-H. Liao, L. Wang, On the low-velocity impact responses of auxetic double arrowed honeycomb, Aerosp. Sci. Technol. 98 (2020) 105698, http://dx.doi.org/10.1016/j.ast.2020.105698.
[49] J. Zhang, G. Lu, Dynamic tensile behaviour of re-entrant honeycombs, Int. J. Impact Eng. 139 (2020) 103497, http://dx.doi.org/10.1016/j.ijimpeng.2019.103497.
[50] X. Cheng, Y. Zhang, X. Ren, D. Han, W. Jiang, X.G. Zhang, H.C. Luo, Y.M. Xie, Design and mechanical characteristics of auxetic metamaterial with tunable stiffness, Int. J. Mech. Sci. 223 (2022) 107286, http://dx.doi.org/10.1016/j.ijmecsci.2022.107286.

[51] T. Baran, M. Öztürk, In-plane elasticity of a strengthened re-entrant honeycomb cell, Eur. J. Mech. A Solids 83 (2020) 104037, http://dx.doi.org/10.1016/j.euromechsol.2020.104037.

[52] X.Y. Zhang, X. Ren, X.Y. Wang, Y. Zhang, Y.M. Xie, A novel combined auxetic tubular structure with enhanced tunable stiffness, Composites B 226 (2021) 109303, http://dx.doi.org/10.1016/j.compositesb.2021.109303.

[53] Y. Zhang, L. Sun, X. Ren, X.Y. Zhang, Z. Tao, Y. Min Xie, Design and analysis of an auxetic metamaterial with tuneable stiffness, Compos. Struct. 281 (2022) 114997, http://dx.doi.org/10.1016/j.compstruct.2021.114997.

[54] Y. Chen, M.-H. Fu, A novel three-dimensional auxetic lattice meta-material with enhanced stiffness, Smart Mater. Struct. 26 (10) (2017) 105029, http://dx.doi.org/10.1088/1361-665X/aa819e.

[55] N. Novak, M. Vesenjak, Z. Ren, Auxetic cellular materials - a review, J. Mech. Eng. 62 (2016) 485–493, http://dx.doi.org/10.5545/sv-jme.2016.3656.

[56] C. Luo, C.Z. Han, X.Y. Zhang, X.G. Zhang, X. Ren, Y.M. Xie, Design, manufacturing and applications of auxetic tubular structures: A review, Thin-Walled Struct. 163 (2021) 107682, http://dx.doi.org/10.1016/j.tws.2021.107682.

[57] K. Wang, R. Cai, Z. Zhang, J. Liu, S. Ahzi, Y. Peng, Y. Rao, Compressive behaviors of 3D printed polypropylene-based composites at low and high strain rates, Polym. Test. 103 (2021) 107321, http://dx.doi.org/10.1016/j.polymertesting.2021.107321.

[58] D. Popescu, A. Zapciu, C. Amza, F. Baciu, R. Marinescu, FDM process parameters influence over the mechanical properties of polymer specimens: A review, Polym. Test. 69 (2018) 157–166, http://dx.doi.org/10.1016/j.polymertesting.2018.05.020.

[59] M. Štaffová, F. Ondreáš, J. Svatík, M. Zbončák, J. Jančář, P. Lepcio, 3D printing and post-curing optimization of photopolymerized structures: Basic concepts and effective tools for improved thermomechanical properties, Polym. Test. 108 (2022) 107499, http://dx.doi.org/10.1016/j.polymertesting.2022.107499.

[60] J. Martín-Montal, J. Pernas-Sánchez, D. Varas, Experimental characterization framework for SLA additive manufacturing materials, Polymers 13 (7) (2021) http://dx.doi.org/10.3390/polym13071147.

[61] W. Chen, B. Song, Split Hopkinson (Kolsky) Bar: Design, Testing and Applications, in: Mechanical Engineering Series, Springer US, 2012.

[62] S. Nemat-Nasser, J.B. Isaacs, J.E. Starrett, Hopkinson techniques for dynamic recovery experiments, Proc. R. Soc. A 435 (1894) (1991) 371–391.

[63] ISO, IEC, ISO, IEC 25010 (2011) 2011.

[64] H. Lei, C. Li, J. Meng, H. Zhou, Y. Liu, X. Zhang, P. Wang, D. Fang, Evaluation of compressive properties of SLM-fabricated multi-layer lattice structures by experimental test and mu-CT-based finite element analysis, Mater. Des. 169 (2019) 107685, http://dx.doi.org/10.1016/j.matdes.2019.107685.